Time evolution of the electron energy distribution function in pulsed microwave magnetoplasma in H2

J. L. Jauberteau, I. Jauberteau, O. D. Cortázar, and A. Megía-Macías

Citation: Physics of Plasmas **23**, 033513 (2016); doi: 10.1063/1.4944677
View online: http://dx.doi.org/10.1063/1.4944677
View Table of Contents: http://scitation.aip.org/content/aip/journal/pop/23/3?ver=pdfcov
Published by the AIP Publishing

Time evolution of the electron energy distribution function in pulsed microwave magnetoplasma in H_2

J. L. Jauberteau,[1,a)] I. Jauberteau,[1] O. D. Cortázar,[2] and A. Megía-Macías[3]
[1]*UMR 7315 CNRS, SPCTS, 12 Rue Atlantis, 87068 Limoges, France*
[2]*Universidad de Castilla-La Mancha, ETSII-INEI, Av. Camilo Jose Cela s/n, 13071-Ciudad Real, Spain*
[3]*ESS Bilbao Consortium, Polígono Ugaldeguren-III Pol. A 7B, 48170-Zamudio, Vizcaya, Spain*

(Received 17 February 2016; accepted 9 March 2016; published online 24 March 2016)

Time evolution of the Electron Energy Distribution Function (EEDF) is measured in pulsed hydrogen microwave magnetoplasma working at 2.45 GHz. Analysis is performed both in resonance (B = 0.087 T) and off-resonance conditions (B = 0.120 T), at two pressures (0.38 Pa and 0.62 Pa), respectively, and for different incident microwave powers. The important effect of the magnetic field on the electron kinetic is discussed, and a critical analysis of Langmuir probe measurements is given. The Electron Energy Distribution Function is calculated using the Druyvesteyn theory (EEDF) and is corrected using the theory developed by Arslanbekov in the case of magnetized plasma. Three different components are observed in the EEDF, whatever the theory used. They are: (a) a low electron energy component at energy lower than 10 eV, which is ascribed to the electron having inelastic collisions with heavy species (H_2, H, ions), (b) a high energy component with a mean energy ranging from 10 to 20 eV, which is generally ascribed to the heating of the plasma by the incident microwave power, and (c) a third component observed between the two other ones, mainly at low pressure and in resonance conditions, has been correlated to the electron rotation in the magnetic field. © *2016 AIP Publishing LLC*. [http://dx.doi.org/10.1063/1.4944677]

I. INTRODUCTION

Magnetized plasmas (magnetoplasmas) are characterized by higher ionization, dissociation, or excitation efficiencies than unmagnetized plasmas, and the understanding of elementary processes produced during the breakdown and decay in pulsed plasmas are of great interest for many applications in plasma processing industry.[1,2] Extensive researches performed in different kinds of reactor with different gaseous mixtures (Ar, N_2, H_2, etc.) have been conducted mainly by means of electrical probes or emission spectroscopy to characterise the plasma parameters at the steady state and to understand or to act on the plasma chemistry.[3–8] In recent works, transient phenomena have been studied by means of several complementary investigation methods (directional coupler for incident and reflected power measurements, VUV (vacuum-ultraviolet) spectroscopy, and Langmuir probe) to investigate the plasma breakdown dynamic in ECR plasma sustained in hydrogen on a microsecond scale.[9–11] The purpose of the present work is to complete these previous studies and to investigate the change of the Electron Energy Distribution Function (EEDF) on the same microsecond scale. Investigations are performed by means of single probes, under off-resonance, and resonance conditions all over the breakdown time until the steady state of the discharge. The study of the plasma decay when the power is switched off gives information about the electron recombination in the hydrogen magnetoplasma. The main goal is to improve the knowledge about the evolution of plasma parameters during pulse mode.

In Secs. III–IV, first, we discuss the single probe measurements performed in magnetized plasma and propose a method to determine the EEDF. Second, we provide and discuss the different results obtained during the ignition or after the stop of the microwave power.

II. EXPERIMENTAL SETUP

The experimental study is made in a plasma source driven by a 3 kW adjustable power magnetron of 2.45 GHz operating at 50 Hz in pulsed mode. Figure 1 shows a cross-section view of the plasma chamber. It is a copper made cylinder with 93 mm length by 90 mm inner diameter including an external water cooling bath for heat removal. Microwave is injected through one side, while the opposite is used as vacuum pumping and diagnostics ports. From the microwave injection side, a brass piece made with internal steps is used as microwave impedance adaptor between the plasma chamber and the WR 330 microwave waveguide. A two-stub tuner is used for fine plasma impedance matching. A 10 mm thickness quartz window separates the vacuum enclosure from the microwave driver system. A set of four coaxial coils arranged in two pancakes with independently variable circulating currents of about 10 A can produce different magnetic field profiles by means of a positioning mechanism. A detailed description is given in Ref. 3 where the synchronization system for the Langmuir probe measurements is also explained. Each point of the I-V characteristic is averaged on 20 data acquisitions performed at the same time in different consecutive plasma pulses. The system acquires each I-V point during 62.5 ns and the acquisition time for a full I-V curve is between 3 and 4 min depending on the voltage range used. Time resolved I-V curve can be obtained by

a)E-mail: jean-louis.jauberteau@unilim.fr

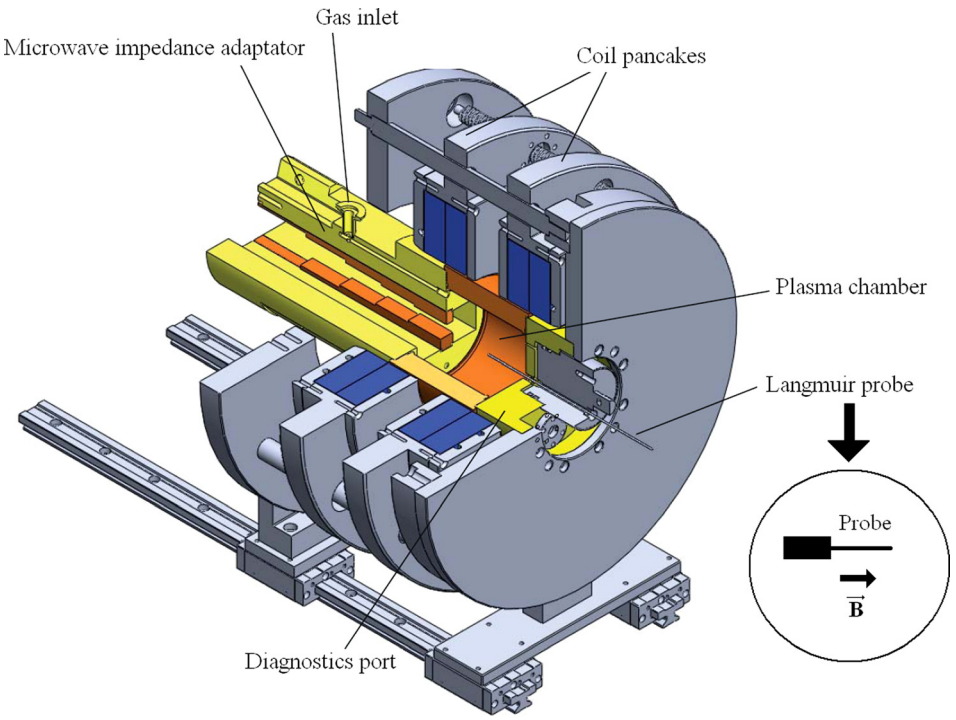

FIG. 1. Cross section view of the plasma source including the plasma chamber and other subsystems.

synchronizing Langmuir probe, trigger driver, and magnetron via a delay generator. Jitter is carefully checked, and the value is kept lower than 200 ns to obtain an accurate time evolution. Full I-V curves are measured at different times during the breakdown process. The incoming power rise time of about 3 μs permits to make clear measurements of the plasma breakdown with respect to the excitation. The Langmuir probe is made of a tungsten wire 6 mm length and 0.5 mm diameter and is located at the center of the plasma chamber and is placed along the magnetic field because of technical reasons. The z-axis magnetic profile has been measured by means of a vector magnetic probe and is given in previous articles.[9,11] It is possible to perform probe measurements for different magnetic field values, moving the probe along the z-axis. The magnetic field increases from 0.087 T to 0.120 T with z increasing from $z = 0$ (at the microwave injection) to $z = 60$ mm downstream the microwave injection and it remains constant from $z = 60$ mm to 90 mm downstream the wave injection side. The Langmuir probe driver is the ESPION system (Hiden Analytical LTD). However, the EEDFs are calculated using our own home-made data treatment software based on the Druyvesteyn theory,[12] assuming isotropic and collisionless plasma around the probe tip. It is corrected in the case of magnetic plasma using methods given in Sec. III of this paper. In these calculations, the second derivative of the I-V probe characteristic is performed using the numerical SHC (Simulation of Harmonic Components) method that we have developed and presented in previous publications.[13,14] The SHC method is particularly efficient to compute and filter numerical derivatives in the case of noisy signals. Figure 2 shows the typical I-V probe characteristics with the corresponding second derivatives. The total current ranges between 0.015 A (when only the electrons are attracted) and −0.01 A (at the ion aturation). The plasma potential (V_p) used as reference to calculate the electron energy is deduced from the crossing point of the second derivative with the x-axis. The EEDF is calculated considering the retardation part of the curve for electrons, i.e., the part corresponding to $V < V_p$.

In H_2 plasma, the main negative ion produced is H^-. It is formed by dissociative attachment of slow electrons ($Te < 2$ eV) to vibrationally excited hydrogen molecules $H_2(v = 4–9)$.[15] In the present work, hydrogen plasma has a mean electron energy ranging from 10 to 20 eV, and the vibrational excitation of $H_2(v = 4–9)$ is probably efficient contrary to the mechanism of dissociative attachment of slow electron producing H^-. Moreover, because of the low affinity (0.75 eV), H^- is quickly destroyed at high power. Consequently, we assume that in our experimental conditions (power ranges from 900 W to 1500 W), negative ion is not produced and the charged particles within the plasma are singly charged positive ions and electrons, only.

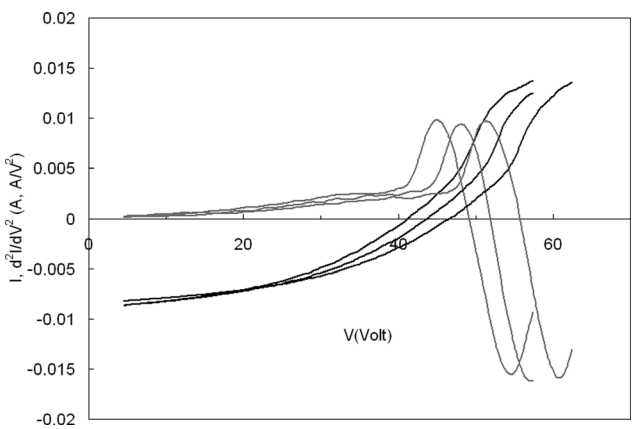

FIG. 2. Typical I-V probe characteristic and second derivative function. Measurements have been performed at B = 0.120 T, P = 0.62 Pa, and 1500 W.

We have studied the EEDF time evolution on a microsecond scale both in off-resonant (B > ECR) (0.120 T) and resonant (B = ECR) (0.087 T) conditions, considering two pressures 0.38 Pa and 0.62 Pa and at different incident powers. The pulse time is fixed equal to 50% of the duty cycle.

III. PROBE THEORY IN MAGNETOPLASMA

When a magnetic field is applied within the plasma, the electron trajectory is wrapped around the magnetic fields lines producing a spiral. The circle corresponding to the spiral projected on the plan perpendicular to the magnetic field has a radius (Larmor radius) given by

$$\rho_e = \frac{m_e v_{e\perp}}{eB}, \tag{1}$$

where $v_{e\perp}$ is the component perpendicular of the electron velocity. According to Fridman,[16] in the case of strong magnetic fields, the Larmor radius plays the same role as the mean free path without magnetic field. At the ECR, assuming a mean electron energy $\langle \varepsilon_e \rangle$ ranging from 10 to 20 eV, the Larmor radius ranges from 1.2×10^{-4} m to 1.7×10^{-4} m and the mean free path in unmagnetized plasma ranges from 6×10^{-2} m at P = 0.38 Pa to 3×10^{-2} m at P = 0.62 Pa. Considering an electron density of about $10^{16}\,m^{-3}$, the Debye length (λ_D) ranges from 1.9×10^{-4} m for $\langle \varepsilon_e \rangle = 10$ eV to 2.7×10^{-4} m for $\langle \varepsilon_e \rangle = 20$ eV. So, the Larmor radius is of the order of the Debye length and the collisionless condition is not exact. Moreover, in these experiments, the probe radius $r_p = 2.5 \times 10^{-4}$ m is lower than the sheath thickness around the probe (typically few λ_D) and we cannot consider a thin sheath. Consequently, the Druyvesteyn theory cannot be rigorously used to measure the EEDF because it assumes a collisionless thin sheath around the collecting probe. A correction of the Druyvesteyn theory is necessary in the case of magnetoplasmas.

A. The electron energy relaxation length

Whatever the theory used to calculate plasma parameters or to measure the EEDF, the Langmuir probes can be used to study the plasma only if the disturbed length by the probe is small in comparison to the electron energy relaxation length λ_ε. This parameter depends on the electron collision cross sections with any other species present in the plasma.[17–20] It is given by

$$\lambda_\varepsilon = \lambda \left(\frac{\nu_m}{\delta \nu_m + \nu^*} \right)^{1/2}, \tag{2}$$

where λ is the electron mean free path in the case of elastic collision, ν_m and ν^* are the elastic and inelastic electron-neutral collision frequencies, and $\delta = 2\frac{m_e}{M}$ is a factor depending on the electron to neutral species mass ratio.

When the characteristic probe disturbed length is very large compared to the electron energy relaxation length, the EEDF measured is due to a local electron kinetic around the probe. The EEDF shape depends mainly on the local heating field and on the collisions produced in the probe disturbed region. So it is not representative of the EEDF bulk plasma. Conversely, when the probe disturbed length is small compared to λ_ε and larger than λ, the electron kinetic is nonlocal, and the EEDF can be considered isotropic because of the dominant elastic collision processes. In these conditions, electron collisions produced in the disturbed length have no significant effect on the whole EEDF measured, which mainly depends on the plasma bulk and on the disturbance due to the drain of electron to the probe.[17–20]

The electron equation for the EEDF has the form of an anisotropic diffusion equation, because the electron diffusion coefficient is a tensor with a radial and longitudinal component through the probe disturbed region. Since the diffusion coefficient has two components, the length of energy relaxation is anisotropic with two components has well. In the direction parallel to the magnetic field, the energy relaxation length is not affected by the magnetic field but it changes in the radial direction because of the increase of the effective mean free path and it becomes[17–20]

$$\lambda_{\varepsilon\perp} = \frac{\lambda_\varepsilon}{\alpha}, \tag{3}$$

with $\alpha = \left[1 + \left(\frac{\omega_c}{\nu_m} \right)^2 \right]^{1/2}$.

The electron motion in the probe disturbed region depends on both radial and longitudinal diffusion components, and the value of the energy relaxation length ranges between the parallel and the radial energy relaxation length values according to the electron trajectory. We will consider the worst case where it is equal to the radial component given by Equation (3). In the case of a cylindrical probe, the region disturbed by the probe is typically

$$r_d = r_s \ln(L/r_s), \tag{4}$$

where r_s is the sheath radius and L is the probe length.[17] Figure 3 shows the change of the ratio of the radial relaxation length to the disturbed probe length ($\frac{\lambda_{\varepsilon\perp}}{r_d}$) versus electron energy in the case of the hydrogen magnetoplasma. The energy relaxation length is calculated using the total cross section values given by Tawara *et al.*[21] It includes elastic and inelastic collisions of electrons with H_2 producing ionization

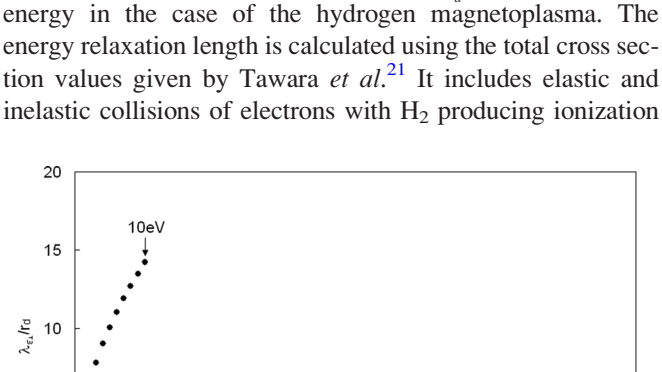

FIG. 3. Ratio of the electron energy relaxation length on the disturbed probe length versus electron energy in H_2 magnetoplasma. The straight line indicates the ratio equal to 1.

or electronic exited states and inelastic collisions of electrons with H, H^+, and H_3^+. For most of these processes, the inelastic collision threshold is less than 16 eV.

It can be seen that the ratio is larger than 1 for electron energy ranging from 0.1 to 30 eV. At electron energy lower than the inelastic collision threshold located between 10 and 16 eV, the collisions are mainly elastic. The ratio $\frac{\lambda_{e\perp}}{r_d}$ increases with electron energy increasing up to 14 at 10 eV. At electron energy larger than the inelastic collision threshold, the ratio drastically decreases up to 2.15 at 16 eV because of the efficiency of inelastic collision processes, which are mainly the $B^3\Sigma_u^+$, $C^1\Pi_u$, and $B^1\Sigma_u^+$ electronic state excitations and the ionization of H_2. At larger electron energy, the ratio slowly decreases with electron energy increasing and becomes lower than 1 at about 30 eV. It is worth noting that for electron energy larger than the threshold value (10 to 16 eV), the electron relaxation length value depends mainly on the inelastic collisions of the electrons with the molecular hydrogen. The other species H, H^+, or H_3^+ have a low effect because of the low density species (<10% H_2 density). As previously published, these results are calculated considering the radial components of the electron energy relaxation length. In the direction parallel to the magnetic field, $\alpha = 1$ in Equation (3) and the energy relaxation length is 2 or 3 orders of magnitude larger than the value obtained for the radial component.

So, in the worst case (radial component), the local electron kinetic regime is not fulfilled all over the EEDF energy range. Nevertheless, the main part of the EEDF (more than 90%) is probably not too much affected by the collisions produced in the region disturbed by the probe. For this reason, we assume in a first approximation that the electron collisions produced in the disturbed length have no significant effect on the EEDF measurements, which mainly depends on the plasma bulk and on the disturbance due to the drain of electron to the probe, i.e., on the diffusion through the disturbed region.

B. Correction of the diffusion through the probe disturb region

A recent theory of the electron probe current collected in the presence of a magnetic field is given in the literature.[22–27] It accounts for the radial and parallel diffusion of electrons through the disturbed region and of course is available in the case of a non-local electron kinetic regime, only. This theory is based on the previous work of Swift[28] concerning the disturbance of the plasma produced by the probe and its consequence on the probe characteristic. The disturbance can be neglected when the electron diffusion rate is high enough to cope with the drain of electrons from plasma to probe. Otherwise, EEDFs are different at the vicinity of the probe and in the undisturbed plasma and a correction is necessary.

Assuming a diffusion regime, the electron probe current depends on a diffusion parameter ψ and is given by

$$I_e(U) = \frac{8\pi eS}{3m^2\gamma}\int_{eU}^{\infty}\frac{(\varepsilon_e - eU)f(\varepsilon_e)d\varepsilon_e}{1+\left((\varepsilon_e - eU)/\varepsilon_e\right)\Psi}, \tag{5}$$

where ε_e is the total electron energy in the sheath, U is the probe potential with respect to the plasma potential, $\psi(\varepsilon_e)$ is the diffusion parameter depending on ε_e, S is the collecting probe area, γ is a geometric factor, and $f(\varepsilon_e)$ is the isotropic distribution function, correlated to the electron density n_e by

$$\int_{\varepsilon e0}^{\infty} f(\varepsilon_e)\sqrt{\varepsilon_e}d\varepsilon_e = n_e, \tag{6}$$

where $\varepsilon_{e0} = eU = 0$. In the present work, the cylindrical probe is located at the middle of the reactor and is parallel to the magnetic field and the diffusion parameter is given by

$$\Psi = \frac{\pi L}{4\gamma\rho_e}. \tag{7}$$

The γ factor can be approximated using $\gamma = 0.71 + \frac{0.25}{x}$, where x is the ratio of the probe to the Larmor radius.[22] In our experimental conditions, Larmor radius and γ factor range from 1.2×10^{-4} m to 1.7×10^{-4} m and from 0.83 to 0.88, respectively.

Using Equation (5), it can be shown that the second derivative of the electron current collected by the probe is given by[22]

$$I''(U) = Cef(eU) - C\int_{eU}^{\infty} K(\varepsilon_e, U)f(\varepsilon_e)d\varepsilon_e, \tag{8}$$

where C is a constant and

$$K(\varepsilon_e, U) = \frac{2\Psi{\varepsilon_e}^2}{\left[\varepsilon_e(1+\Psi) - \Psi eU\right]^3}. \tag{9}$$

A similar equation can be obtained, in the case of the first derivative of the electron current using also Equation (5). Equation (8) shows that the EEDF is proportional to the second derivative of the I-V probe characteristic in the retarding region only if the second term of Equation (8) (the integral term) can be neglected compared to the first one. This means that the plasma potential can be measured at the zero crossing point of the second derivative with the x-axis only if the second term in Equation (8) (the integral part) can be neglected when the probe is biased at the plasma potential.

In previous works,[22–27] considering Equation (5), the authors have shown that according to the diffusion parameter value, the EEDF can be approximated using the first or the second derivative of the collected current. In the present work, we propose a new algorithm to correct the Druyvesteyn method using Arslanbekov theory (Equation (8)), without any approximation according to the ψ value. The method is as follows:

First, the EEDF is calculated using the Druyvesteyn equation and second, by means of successive adjustments of the previous distribution function, we correct the EEDF in order to obtain a perfect agreement between the experimental second derivative and the calculated one using Equation (8). In these conditions, the EEDF obtained is the solution of Equation (8) and the correction of the EEDF taking into

account the diffusion through the probe disturbed region is fulfilled all over the electron energy range. The integral part of Equation (8) is calculated by means of a Monte Carlo integration method.

Figure 4 compares the EEDF calculated using the Druyvesteyn theory with the corrected EEDF calculated using the previous algorithm. The figure also compares the experimental second derivative with the calculated using Equation (8), considering the corrected EEDF. In this example, the pressure is 0.62 Pa and the power is 900 W and B = 0.120 T. It can be seen that the EEDF calculated using the Druyvesteyn theory is lower than the one calculated with the Arslanbekov theory. The difference is more important at high electron energy than below 10 eV.

This difference between the two theories is systematic whatever the pressure and the power are and the relative error between the two theories increases with the magnetic field increasing. When the integral term of Equation (8) can be neglected, i.e., at large electron energy and at electron energy lower than 10 eV, the two theories give the same results whatever the magnetic field is. At B = 0.087 T and at electron energy lower than 16 eV, the difference between the EEDF values calculated using the two theories is of the order of the experimental error (10%–15%). At B = 0.120 T, the difference is more important and can be equal to 30% at 16 eV and even more for larger electron energies in the EEDF tail, as shown in the examples displayed in Figure 5.

It is worth noting that because of the small difference observed at low electron energy between the EEDF values calculated using the two theories, the error on the plasma potential value measured at the zero crossing point of the second derivative of the probe characteristic with the x-axis is probably low.

These first results show that the Druyvesteyn theory gives underestimated values compared to the Arslanbekov theory, mainly at large magnetic field values. Nevertheless, it gives good results in resonance conditions on the main part of the EEDF before 10 eV when the non-local electron kinetic regime can be considered.

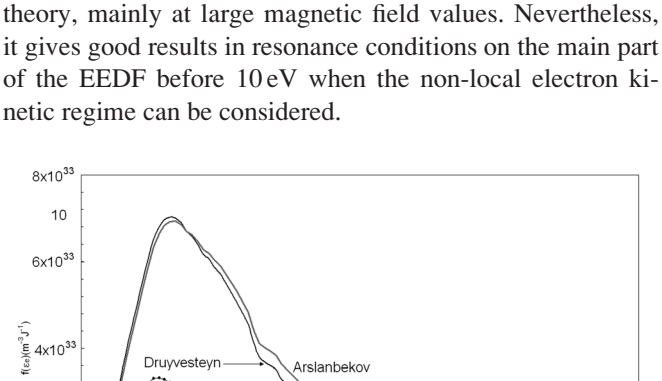

FIG. 4. Comparison of EEDF calculated with the Druyvesteyn and the Arslanbekov theories. Measurements have been performed at 0.62 Pa, 900 W with a magnetic field B = 0.120 T. Also, the figure compares the experimental second derivative to the calculated one using Equation (8) and considering the corrected EEDF (Arslanbekov).

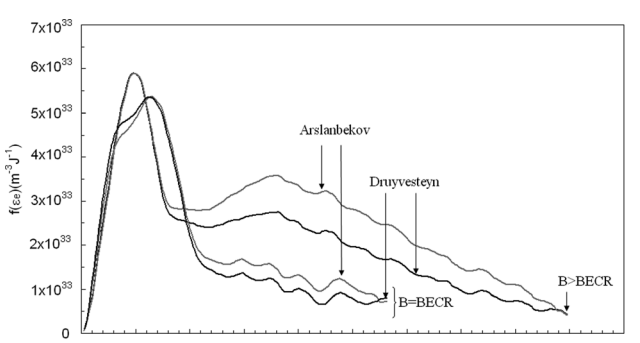

FIG. 5. Comparison of EEDF measured using the Druyvesteyn and the Arslanbekov theories. Measurements have been performed at low pressure (0.62 Pa, at 0.087 T and B = 0.120 T.

IV. EEDF ANALYSIS IN THE MAGNETOPLASMA

A. Electron density and mean electron energy

Figures 6(a) and 6(b) display the electron density and the mean energy versus the incident power, respectively. Measurements are performed at t = 300 μs after the discharge

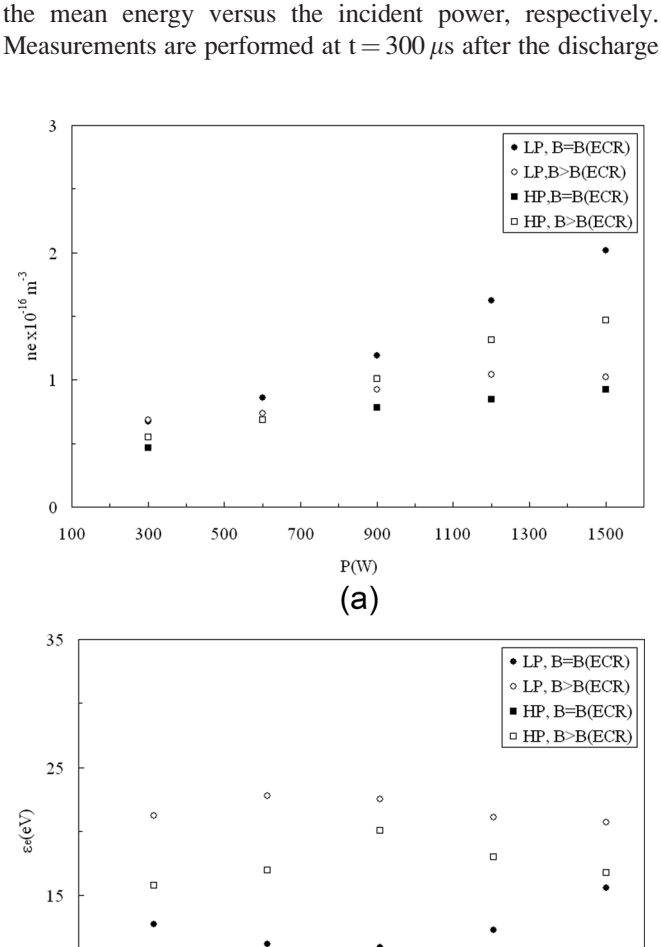

FIG. 6. Electron density (a) and mean energy (b) versus incident power, in resonance (B = B(ECR) and off resonance (B > B(ECR) conditions, at the two pressures LP (0.38 Pa) and HP (0.62 Pa) and at t = 300 μs.

ignition. Values are calculated using numerical integrations over the EEDF (Equation (6))[13,14] and considering the two pressures under investigation, in and off-resonance conditions. It can be seen that the electron density increases and the electron energy remains nearly unchanged versus increasing power. At low pressure, the electron density obtained in the resonance condition is larger than the one measured off-resonance conditions contrary to the measurements performed at high pressure, which agree with Cui and Boswell results.[29] The difference observed at low pressure between Cui and our results could be ascribed to the change in excitation frequency, which is 2.45 GHz in our work and ranges from 20 to 60 MHz in Cui's experiments. In the case of the electron energy, the value measured in resonance conditions is lower than the value measured off resonance at low and high pressures. This agrees with Cui and Boswell results.[29] Moreover, we observe that the plasma potential is generally lower in resonance conditions (30 V to 45 V) than in off-resonance conditions (40 V to 65 V).

In the reactor, the plasma heating results in the electromagnetic wave interaction with the plasma. In a first approximation, the microwave is a transverse electromagnetic wave propagating along the static magnetic field, produced in the reactor by the coil pancakes. The theory shows that the electron motion remains transverse like the electric field. The study of the wave dispersion[30] shows that at these electron densities (see Figure 6) and at a microwave frequency of 2.45 GHz, the low frequency branch of the Right Hand Circularly Polarized waves (RHCP), i.e., the whistler waves and the Left Hand Circularly Polarized waves (LHCP) can propagate in and off-resonance conditions. The Electron Cyclotron Resonance (ECR), at the 2.45 GHz frequency, is obtained when the magnetic field is equal to 0.087 T. It corresponds to the resonance of the RHCP wave at $\omega = \omega_c$.[30]

In Secs. IV B and IV C of this article, we study the change of EEDF profile versus time and plasma parameters, during the plasma ignition until the steady state. This study supposes that there is no interaction between the polarised probe and the discharge acting on the plasma ignition. In a previous work, diagnostic performed by means of emission spectroscopy analysis on the VUV Lyman band (maximum at 160 nm) and Lyman-α band (121.6 nm) shows a qualitative agreement between the VUV light and the Langmuir probe data (T_e, n_e). This correlation between probe measurements and this non intrusive diagnostic method (VUV spectroscopy) agrees with our assumption.[31]

B. Time evolution of the EEDF under off-resonance conditions

Figure 7 displays the time evolution of the EEDF measured under off-resonance conditions, at high pressure (0.62 Pa), with an incident power equal to 1500 W and a magnetic field intensity B = 0.120 T. It can be seen that from 6 μs to 300 μs, the EEDF shape remains nearly unchanged. However, the position of the maximum of the curve fluctuates at the beginning of the breakdown from 6 μs to 40 μs and is finally stabilized for larger times. This first step until 40 μs corresponds to the change of plasma coupling at the beginning of the plasma formation[9] and can be correlated to the temperature peaking already observed at low times after the plasma ignition.[3] The steady state is typically obtained 40 μs after the ignition. As shown in Figures 7 and 8, the EEDF is composed of two components, which can be fitted using the generalized Maxwell distribution form[32–35]

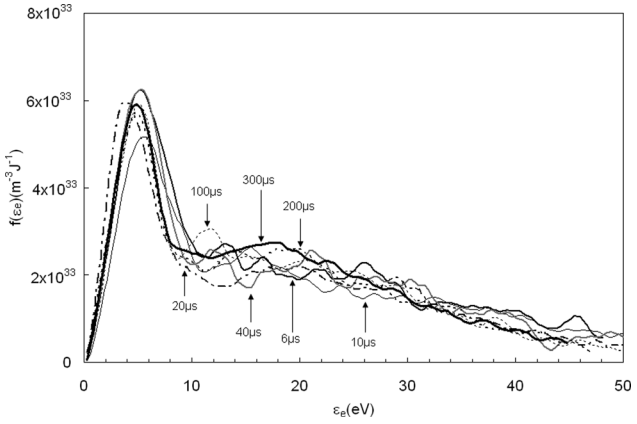

FIG. 7. EEDF, measured for different times after the discharge ignition. Measurements are performed at 1500 W, 0.62 Pa, and B = 0.120 T.

$$f(\varepsilon_e) = C\sqrt{\varepsilon_e}\exp\left(-\left(\frac{\varepsilon_e}{a}\right)^k\right), \tag{10}$$

where, k, a, C are the constant values of real types.

(a) One component is the high energy tail of the distribution. As shown in Figure 8, it corresponds to a Maxwell-Boltzmann distribution with Te = 19 eV. This component corresponds to the plasma electron heating due to the microwave excitation. Generally, in the case of ionized gases at high frequency, it is described by a Margenau distribution function given by[36]

$$f(\varepsilon_e) = \sqrt{\varepsilon_e}\exp(-P(\varepsilon_e)), \tag{11}$$

with $P(\varepsilon_e) = b\varepsilon_e^2 + c\varepsilon_e$, $b = \frac{6m_e}{M\varepsilon_2^2}$, $c = 2b\varepsilon_1$, $\varepsilon_2 = eE\lambda$, and $\varepsilon_1 = \frac{1}{2}m(\omega\lambda)^2$, where M, e, m_e, λ, and ω are the mass of gas, the electron charge and mass and the electron mean free path, and the angular frequency, respectively. It can be seen

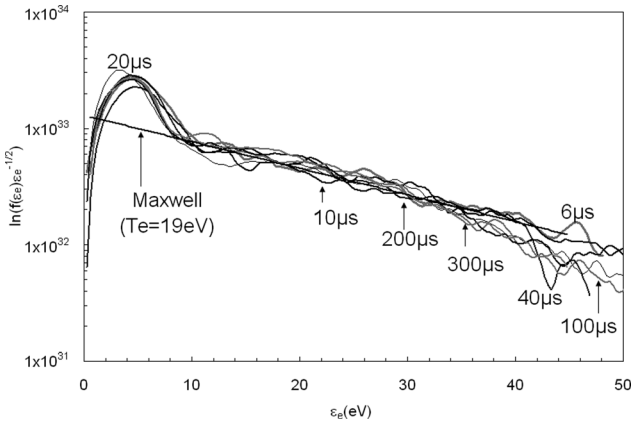

FIG. 8. $\ln(f(\varepsilon_e)\varepsilon_e^{-1/2})$ versus electron energy, comparison with a Maxwell-Boltzmann distribution with (Te = 19 eV).

from the above equation that if b is low (typically $<10^{-7}$, for ε_e given in eV unit), the first term of $P(\varepsilon_e)$ can be neglected for ε_e lower than 100 eV. In this condition, the Margenau distribution is equivalent to a Maxwell-Boltzmann distribution function. Such low b value is obtained for a large local electric field ($>1.8 \times 10^5$ V/m). In our experiments, the electric field in the reactor has been estimated as ranging from 10^5 to 4.5×10^5 V/m.[11] This could explain the Maxwell-Boltzmann profile observed.

(b) The other one is the low energy component which has the parameters a and k in Equation (10) ranging from 5 to 10, according to the experimental conditions. It corresponds to a sharp distribution components located at energy lower than 10 eV. This component is probably due to the inelastic collisions of electron with heavy species in which efficiency is increased because of the magnetic field. In a first approximation, the R ratio of these two component areas (a) and (b) gives a rough estimation of the electron energy transfer efficiency from electrons to the heavy particles. R is about 1.02, in the case of results displayed in Figure 7. This parameter will be used in Sec. IV C to compare results obtained in different experimental conditions.

At lower pressure (0.38 Pa) and in off-resonance conditions (B = 0.120 T), the signal measured (not shown here) is more fluctuating. The EEDFs are smaller, but the shape remains the same with always the two components. The R ratio (R = 0.206) is smaller at low pressure than at high pressure, because of the decrease of the inelastic collisions. Figure 9 shows the EEDF measured at the steady state at this low pressure and at 1500 W. It can be seen that the shape is the sum of the two components A (with $k = \alpha = 6$ in Equation (10)) and B, the Maxwellian with $T_e = 13$ eV in that case.

1. Study of the electron recombination process.

Looking at the decay of the A component when the discharge is switched off, it is possible to determine the electron recombination rate constant within the hydrogen plasma. Figure 10 shows the change of electron density versus time while the decay after the stop of the incident microwave power initially at 1500 W. Measurements are performed at the two pressures 0.38 Pa and 0.62 Pa. It can be seen that the two decays are similar and can be described by means of an exponential curve. The electron decay is due to the reaction of electron in the plasma bulk that can be described by a global process proportional to the hydrogen density and to the electron diffusion to the reactor wall. The global phenomena can be written as

$$\frac{dn_e}{dt} = -k\, n_e n_{H2} + D\nabla^2 n_e. \tag{12}$$

Because of the magnetic field, the radial diffusion to the wall is drastically decreased compared to the diffusion in unmagnetized plasma,[17–20] and it can be neglected compared to the reactive part in Equation (12). So, in a first approximation, the electron density can be written as

$$n_e = n_{e0} \exp(-k\, n_{H2} t). \tag{13}$$

Using this equation and considering data shown in Figure 10, we have determined a global electron recombination rate constant equal to 1.4×10^{-15} m^3 s^{-1} and 2×10^{-15} m^3 s^{-1} at 0.38 Pa and 0.62 Pa, respectively. According to de Graaf *et al.*[37] the fast recombination of electron can be explained considering a two steps mechanism. First, a charge transfer between H_2 vibrationally excited ($v \geq 4$) and a proton

$$H_2(v \geq 4) + H^+ \rightarrow H_2^+ + H. \tag{1}$$

Second, the reaction of the molecular ion formed in reaction (1) with an electron. This reaction can be the direct recombination dissociation

$$H_2^+ + e \rightarrow H + H, \tag{2}$$

or a recombination after formation of H_3^+

$$H_2^+ + H_2 \rightarrow H_3^+ + H \tag{3}$$

and

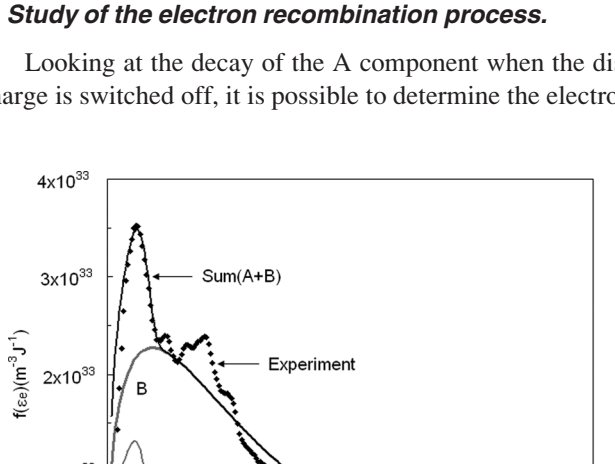

FIG. 9. The two components of the EEDF compared to the experimental EEDF. Measurements are performed at 1500 W, P = 0.38 Pa, B = 0.120 T, and 300 μs after the discharge ignition. A is given by Equation (10) with a = k = 6, B is a Maxwell-Boltzmann distribution with Te = 13 eV.

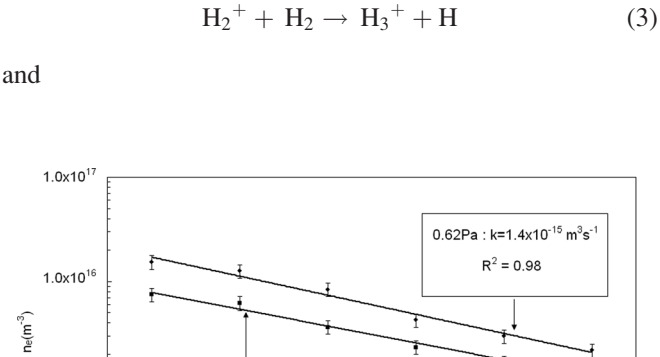

FIG. 10. Electron density decay after the discharge is switched off. Measurements are performed versus time at 0.38 Pa and 0.62 Pa, 0.120 T. The initial incident power is 1500 W.

$$H_3^+ + e \rightarrow 3H \quad (4)$$

or

$$H_3^+ + e \rightarrow H_2(v, J) + H. \quad (5)$$

Reaction (4) is less probable than Reaction (5). Thus, two electron recombination mechanisms are possible in hydrogen plasma, the first is (1), (2) and the second is (1), (3), (5). According to Phelds,[38] the dominant cross section for low energy collision of H_2^+ in H_2 is that for the formation of $H_3^+ + H$. At a relative kinetic energy ranging from 0.1 eV to 1 eV, the cross section ranges from 78×10^{-20} m^2 to 22.7×10^{-20} m^2, this corresponds to reaction rate constants ranging from 1.7×10^{-15} m^3 s^{-1} to 2.2×10^{-15} m^3 s^{-1}, respectively. These values are of the same order that the ones determined from data shown in Figure10 and are close to the value determined considering the Langevin charge-transfer approximation, which is 2.5×10^{-15} m^3 s^{-1}. This suggests that in these experiments the charge-transfer reaction (3) is the limiting step of the dominant electron recombination process (mechanisms (1), (3), (5)). However, the dominant electron recombination process can change with the main hydrogen ion produced in the discharge (H^+, H_2^+, or H_3^+) which seems strongly depending on the experimental conditions.[39]

C. Time evolution of the EEDF under resonance conditions

As previously explained, the electron cyclotron resonance (ECR) condition is fulfilled when the magnetic field is equal to 0.087 T. Figures 11 and 12 display the time evolution of the EEDF measured at 1500 W, under resonance conditions at high and low pressures, respectively. The EEDF shapes are drastically changed compared to the previous ones measured in off-resonance conditions. A third energy component strongly appears between the two previous ones, especially at low pressure, with a peak at electron energies ranging from 10 to 15 eV. The steady state is obtained for longer times than previously under off-resonance conditions, i.e., for times larger than 50 μs at low pressure and for times larger than 150 to 200 μs at high pressure. This agrees with

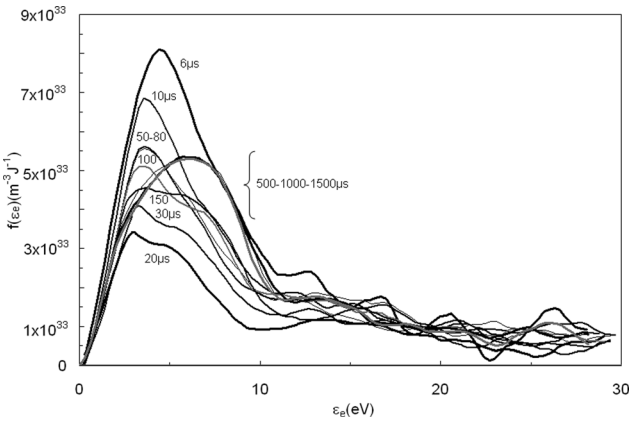

FIG. 11. EEDF, measured at different times after the discharge ignition. Measurements are performed at 1500 W, 0.62 Pa, and B = 0.087 T.

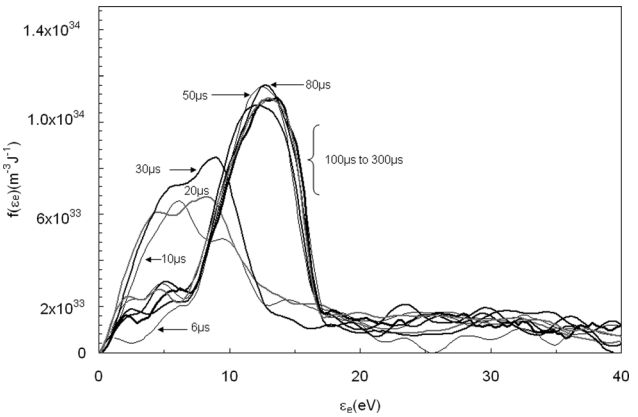

FIG. 12. EEDF, measured at different times after the discharge ignition. Measurements are performed at 1500 W, 0.38 Pa, and B = 0.087 T.

previous results observed in the same experimental conditions.[9] The high energy component tail corresponding to the Maxwell distribution is now drastically decreased compared to the two other components. Assuming now that R is the sum of the two lower energy components on the Maxwell component, its value changes with times and pressure. At high pressure, it ranges from 0.4 to 0.7 for times ranging from 10 μs to 300 μs, and at low pressure, it is equal to 1.69 at 14 μs, 1.71 at 30 μs, and ranges from 0.8 to 1 above 60 μs. The decrease of R for times upper than 60 μs can be explained by the low energy component, which is now drastically vanishing. The EEDF is formed by the two energy components, the new one and the Maxwell-Boltzmann component (with Te = 12 eV).

It is worth noting that the new energy component can also be weakly detected under off-resonance conditions and at low pressure. It could be observed on the side of the low energy component of the EEDF (between 10 and 15 eV) shown in Figure 9.

This new energy component is mainly observed in resonance condition ($\omega = \omega_c$). It is worth noting that the energy of electrons rotating in a resonant magnetic field at 2.45 GHz, ranges from 6.7 eV to 15.1 eV for a Larmor radius ranging from 1×10^{-4} m to 1.5×10^{-4} m. These values are similar to the mean energy of electron in this component.

The behaviour of the three different energy components has been studied at different incident powers. Figures 13–15 compare the EEDF shapes measured at low and high pressures under off-resonance and in resonance conditions for three incident powers: 1500 W, 1200 W, and 900 W, respectively. Measurements have been performed at the steady state, 300 μs after the start of the discharge. It can be seen that under ECR conditions and low pressure, the new energy component becomes dominant compared to the Maxwell-Boltzmann component and that the low energy component disappears at 1500 W. This one appears at high pressure and at 1500 W under ECR conditions, because of the increase of electron-neutral collisions. At power lower than 1500 W (Figures 14 and 15) and at low pressure, the low energy component is mixed to the new one under the resonance conditions. At B = 0.120 T, the EEDF is lower than previously, and the low energy component is observed only at high

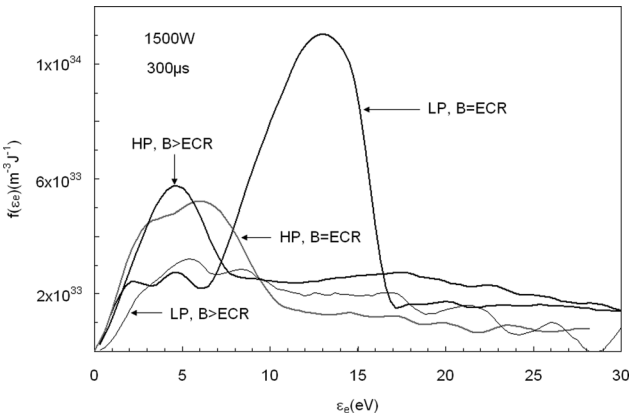

FIG. 13. Comparison of EEDFs measured at 300 μs, 1500 W. At 0.38 Pa and 0.62 Pa, in resonance (B = 0.087 T) and off-resonance (B = 0.120 T) conditions.

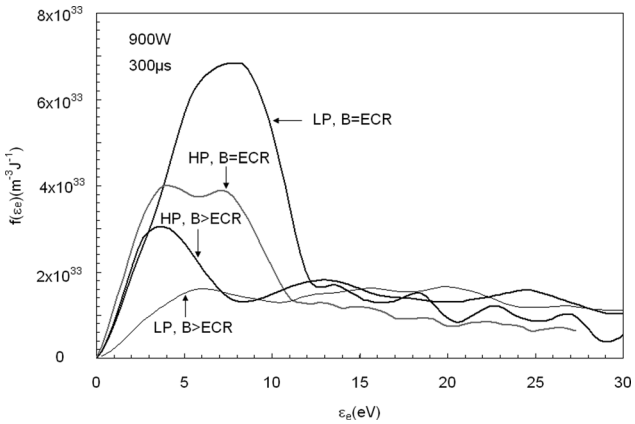

FIG. 15. Comparison of EEDFs measured at 300 μs, 900 W. At 0.38 Pa and 0.62 Pa, in resonance (B = 0.087 T) and off-resonance (B = 0.120 T) conditions.

pressure. Only the Maxwell-Boltzmann component is observed at low pressure for this magnetic field intensity.

At low pressure and 1500 W, the new component increases with increasing time after the plasma ignition until 60 μs then it is dominant and it remains nearly unchanged from 60 μs to 300 μs. The mean electron energy corresponding to this component has been calculated removing the two other components from the total EEDF shape. It increases and ranges from 9 and 15 eV for times increasing from 18 μs to 60 μs after the plasma ignition.

As previously published, the new component is dominant at low pressure and high power under ECR conditions and seems to be correlated to the electron rotating in the plane perpendicular to the magnetic field.[30] However, the phenomenon producing this component is probably more complex and cannot be explained considering only the transverse wave propagating in the infinite plasma. The boundary conditions on the reactor wall have probably an important effect on the EEDF shape and must be taken into account. So, an electron kinetic model, considering collision, heating processes, and wave propagation in the cavity is necessary to understand the change of the EEDF with experimental conditions. Moreover, as previously suggested by Cui and Boswell,[29] Trivelpiece-Gould

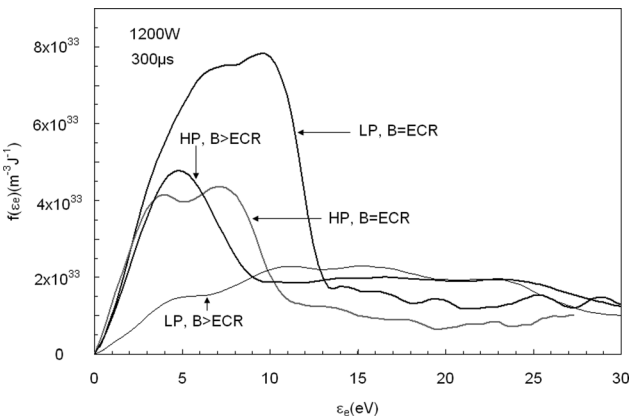

FIG. 14. Comparison of EEDFs measured at 300 μs, 1200 W. At 0.38 Pa and 0.62 Pa, in resonance (B = 0.087 T) and off-resonance (B = 0.120 T) conditions.

electrostatic waves[40] can also propagate and also contribute to the plasma dynamic.

V. CONCLUSION

The time evolution of the EEDF has been investigated in a microwave discharge sustained in a magnetic field, under off-resonance and resonance conditions (ECR), from the start of the discharge to the steady state. Because of the increase in the collision frequency due to the magnetic field, the non-local regime of the kinetic electron is discussed. The study shows that in the present work, only electrons of the EEDF tail with energy larger than 30 eV have a relaxation length smaller than the probe disturbed region. This corresponds to less than 10% of the total EEDF. For this reason, we assume in a first approximation that the non-local regime condition, necessary for probe measurements, is fulfilled over the main part of the EEDF. In this condition, probe measurements are mainly disturbed by the drain of electrons to the probe. This effect can be corrected using the theory given by Arslanbekov. We have compared the results obtained using the Druyvesteyn and this new theory. It appears that the Druyvesteyn theory can be used under our experimental conditions especially at 0.087 T, the correction on the EEDF is low compared to the experimental errors at electron energy lower than 15 eV for B = 0.087 T and lower than 10 eV for B = 0.120 T. It is more significant for electron energy ranging from 20 to 40 eV. However, this energy range concerns a small part of the total EEDF, where the electron kinetic is in a transition region between local and non-local regime and measurements performed at these electron energies are probably perturbed by the probe, because of the short electron energy relaxation length.

EEDF measurements are obtained under various experimental conditions and are compared. Three different components are observed in the EEDF profile:

(1) At $\varepsilon_e < 10$ eV, the low electron energy component, which increases with increasing pressure. It can be ascribed to the electron colliding with the heavy species. The study of this component during the discharge decay after the stop of the incident power shows that the electrons

mainly recombine with H_3^+ and the charge transfer of H_2^+ to H_2 producing H_3^+ is the limiting step of the recombination process.

(2) The high energy component, which can be fitted by a Maxwell-Boltzmann distribution (corresponding also to a Margenau distribution at large electric field ($E > 1.8 \times 10^5$ V/m). This component is ascribed to the heating of electron by the microwave electric field.

(3) A third and intermediate component, mainly observed at B = ECR and at low pressure. It corresponds to a mean electron energy ranging from 9 eV to 15 eV and seems correlated to the electron gyration within the magnetized plasma.

In such a reactor, the wave propagation depends on the boundary conditions and consequently on the reactor geometry and both electromagnetic and electrostatic waves can contribute to the plasma dynamic. A model of the electron kinetic must be done in order to understand the change of the EEDF shape and the formation of this third intermediate component, versus experimental parameters.

[1]S. Gammino, L. Celona, G. Ciavola, F. Maimone, and D. Mascali, Rev. Sci. Instrum. **81**, 02B313 (2010).
[2]J. Pelletier and A. Anders, IEEE Trans. Plasma Sci. **33**, 1944–1959 (2005).
[3]O. D. Cortázar, A. Megía-Macías, and A. Vizcaíno-de-Julián, Rev. Sci. Instrum. **83**, 103302 (2012).
[4]T. Fujimoto, S. Miyachi, and K. Sawada, Nucl. Fusion **28**, 1255–1263 (1988).
[5]T. Ropponen, O. Tarvainen, I. Izotov, J. Noland, V. Toivanen, D. Machicoane, G. Leitner, H. Koivisto, T. Kalvas, O. Peura, P. Jones, V. Skalyga, and V. Zorin, Plasma Sources Sci. Technol. **20**, 055007 (2011).
[6]O. Tarvainen, T. Ropponen, V. Toivanen, J. Ärje, and H. Koivisto, Plasma Sources Sci. Technol. **18**, 035018 (2009).
[7]H. Backer, J. W. Bradley, P. J. Kelly, and R. D. Arnell, J. Phys. D: Appl. Phys. **34**, 2709–2714 (2001).
[8]C. Lyneis, J. Benitez, D. Leitner, N. Noland, M. Strohmeier, H. Koivisto, and O. Tarvainen, in *Proceedings of ECRIS 2010*, edited by T. Thuillier (Grenoble, France, 2010), pp. 162–164.
[9]O. D. Cortázar, A. Megía-Macías, and A. Vizcaíno-de-julián, IEEE Trans. Plasma Sci. **40**(12), 3409–3419 (2012).
[10]O. D. Cortázar, A. Megía-Macías, A. Vizcaíno-de-julián, O. Tarvainen, J. Komppula, and H. Koivisto, Rev. Sci. Instrum. **85**, 02A902 (2014).
[11]O. D. Cortázar, A. Megía-Macías, O. Tarvainen, A. Vizcaíno-de-julián, and H. Koivisto, Plasma Sources. Sci. Technol. **23**, 065028 (2014).
[12]M. J. Druyvesteyn, Z. Phys. **64**, 781–798 (1930).
[13]J. L. Jauberteau and I. Jauberteau, Meas. Sci. Technol. **18**, 1235–1249 (2007).
[14]J. L. Jauberteau and I. Jauberteau, Rev. Sci. Instrum. **78**, 043501 (2007).
[15]F. Taccogna, R. Schneider, S. Longo, and M. Capitelli, Phys. Plasmas **14**, 073503 (2007).
[16]A. Fridman, *Plasma Chemistry* (Cambridge University Press, Cambridge, 2008), p. 150.
[17]L. D. Tsendin, Phys.-Usp. **53**(2) 133–157 (2010).
[18]U. Kortshagen, Phys. Rev E **49**(5), 4369–4380 (1994).
[19]D. H. Kim, C. M. Ryu, S. H. Lee, and J. K. Lee, J. Korean Phys. Soc. **54**(1), 317–322 (2009).
[20]S. J. You and H. Y. Chang, Phys. Plasmas **13**, 043503 (2006).
[21]H. Tawara, Y. Itikawa, H. Nishimura, and M. Yoshino, J. Phys. Chem. Ref. Data **19**(3), 617–636 (1990).
[22]R. R. Arslanbekov, N. A. Khromov, and A. Kudryavtsev, Plasma Source Sci. Technol. **3**, 528–538 (1994).
[23]V. I. Demidov, S. V. Ratynskaia, R. J. Armstrong, and K. Rypdal, Phys. Plasmas **6**, 350–358 (1999).
[24]S. V. Ratynskaia, V. I. Demidov, and K. Rypdal, Rev. Sci. Instrum. **73**(12), 4232–4236 (2002).
[25]V. I. Demidov, S. V. Ratynskaia, and K. Rypdal, Rev. Sci. Instrum. **73**(10), 3409–3439 (2002).
[26]T. K. Popov, P. Ivanova, M. Dimitrova, J. Kovačič, T. Gyergyek, and M. Čerček, Plasma Sources Sci. Technol. **21**, 025004 (2012).
[27]T. K. Popov, M. Dimitrova, F. M. Dias, V. N. Tsaneva, N. A. Stelmashenko, M. G. Blamire, and Z. H. Barber, J. Phys.: Conf. Ser. **44**, 60–69 (2006).
[28]J. D. Swift, Proc. Phys. Soc. **79**, 697–701 (1962).
[29]C. Cui and R. W. Boswell, Appl. Phys. Lett. **63**, 2330–2332 (1993).
[30]*Microwave Excited Plasmas*, Plasma Technology 4, edited by M. Moisan and J. Pelletier (Elsevier, Amsterdam, 1992), pp. 181–212.
[31]O. D. Cortázar, J. Komppula, O. Tarvainen, A. Megía-Macías, A. Vizcaíno-de-Julián, and H. Koivisto, Plasma Sources Sci. Technol. **22**, 015026 (2013).
[32]A. Vasil'eva, High-Temp. **12**(3), 405–412 (1974).
[33]J. Rohmann and S. Klagge, Contrib. Plasma Phys. **33**, 111–123 (1993).
[34]J. L. Jauberteau and I. Jauberteau, Contrib. Plasma Phys. **51**(10), 944–954 (2011).
[35]A. P. Ershov, V. A. Dovzhenko, A. A. Kuzovnikov, and S. N. Oks, Sov. J. Plasma Phys. **7**, 334 (1981).
[36]H. Margenau, Phys. Rev. **69**(9), 508–513 (1946).
[37]M. J. de Graaf, R. Severens, R. P. Dahiya, M. C. van de Sanden, and D. C. Schram, Phys. Rev. E **48**, 2098–2102 (1993).
[38]A. V. Phelds, J. Chem. Phys. Ref. Data **19**, 653–675 (1990).
[39]O. D. Cortázar, A. Megía-Macías, O. Tarvainen, T. Kalvas, and H. Koivisto, Rev. Sci. Instrum. **87**, 02A704 (2016).
[40]A. W. Trivelpiece and R. W. Gould, J. Appl. Phys. **30**, 1784–1793 (1959).